2014 IEEE International Conference on Robotics & Automation (ICRA)
Hong Kong Convention and Exhibition Center
May 31 - June 7, 2014. Hong Kong, China

Kinematic Modeling and Control of a Multi-joint Soft Inflatable Robot Arm with Cable-Driven Mechanism

Ronghuai Qi, Tin Lun Lam, and Yangsheng Xu

Abstract— **In this paper, the kinematic modeling and control for a multi-joint inflatable robot arm with cable-driven mechanism are proposed. The soft inflatable robot arm is capable of imitating human arms to realize remote interaction. The weight of the arm is only about 50 grams, and collision safe. To solve the challenge problems of kinematics of the soft inflatable arm, new approaches are proposed, including redundant rigid arm and soft inflatable joint models. The approaches have a good advantage of applying to muti-joint arms. As our knowledge it is the first time to solve the kinematics of muti-joint soft inflatable arm in Three-Dimensional coordinate space.**

Numerous experiments have been conducted, including movement space and positioning accuracy. The workspace and velocity are close to an adult's arm movement space and normal motion speed.

I. INTRODUCTION

Soft inflatable arms or robots are new research topics in recent years. As they have many advantages and desirable properties. For instance, they are composed of fabric and basic pneumatic parts (eg. an air supply, valves, and tubing). The manufacturing cost can be very low. In addition, they are naturally compliant, which makes them human-safe [1-3]. However, the control issue is challenging. As there are no revalue joints (and hence no joint encoders) for kinematics, and there is currently no built-in force sensor [4-6]. Some researchers did investigations on them. Siddharth Sanan [7-9] developed a soft robot arm, which weights up to 500 grams and has 2DOF, and can be moved only in a plane by driving two cables. Otherlab [10] designed another inflatable walking elephant called Ant-Roach. This robot used textile-based, inflatable actuators that contract upon inflation into specially-designed shapes to effect motion. Since these robots are built out of lightweight fabric-and-air structural members and powered via pneumatics or hydraulics, they exhibited large strength-to-weight ratios. Otherlab [10] seems focus on payload target, since Ant-Roach is less than 32 kilograms but can probably support up to about 454 kilograms. Otherlab developed another inflatable robot arm [10], which is a lightweight, low-cost inflatable robotic arm. The arm weighs is about 2 kilograms and is still able to lift several hundred pounds with just about 400 kPa. Saul [11] designed another inflatable walking elephant. He involved to use compressed air to drive mechanical motion. These robots or arms can be moved by controlling air supply, valves, and tubing. However, there are no clear descriptions about their kinematics models or control algorithms. Although Siddharth Sanan [7-9] designed a inflatable arm and could move in a coordinate system, he seemed not to develop soft inflatable joint models in Three-Dimensional coordinate space.

Fig. 1. The telepresense robot

In this paper, we mainly focus on solving the challenge problems of kinematic modeling and control for a multi-joint inflatable robot arm with cable-driven mechanism. To evaluate the performances and demonstrate the application of the novel inflatable arm, two arms are installed on a telepresense robot, which are shown in Fig. 1. The soft inflatable arm can be moved by pulling six cables installed in shoulder joint and elbow joint. It is only about 50 grams in weight, and can work only in 7.32 ± 3.45 kPa in pressure. It requires less pressure and has lighter weight. Meanwhile, new approaches are proposed to solve the challenge problems of kinematics, which includes 4DOF redundant rigid arm modeling and kinematics, soft inflatable joint modeling and kinematics. These models and algorithms can apply to muti-link soft inflatable arms. Numerous experiments have been conducted, including movement space and positioning accuracy in Three-Dimensional coordinate system.

In Section II, hardware design and implementation are proposed. In Section III, modeling and kinematics are proposed for the soft inflatable arm. In Section IV, the experiments and results are proposed. Finally, the contributions of the current

This work is supported in part by the Smart China Research Project (HK201305001).

Ronghuai Qi and Tin Lun Lam are with the Intelligent Robotics Research Centre, Smart China Research, Smart China Holdings Limited, Shatin, N.T., Hong Kong {ronghuai.qi, tinlun.lam}@smartchinaholdings.com

Yangsheng Xu is with the Dept. of Mechanical and Automation Engineering, The Chinese University of Hong Kong, Shatin, N.T., Hong Kong ysxu@mae.cuhk.edu.hk

work and future work are concluded in section V.

II. HARDWARE DESIGN AND IMPLEMENTATION

The proposed soft inflatable arm is shown in Fig. 2. The structure (including upper arm, lower arm, shoulder joint, and elbow joint) is based on Thermoplastic Polyurethane (TPU), which is a very common, low cost, and environmental friendly inflatable material. The length of upper arm and lower arm are 190mm and 190mm. The shape of shoulder joint and elbow joint are cambers, with middle section diameter 40mm, and both ends diameters 70mm. The thickness of the soft inflatable is 0.18mm, and the weight is only about 50 grams. The joint can be driven by three cables (diameter is 0.3mm) installed in the shoulder joint and elbow joint, respectively. Each cable in the arm pass though shoulder driven tubes, and elbow driven tubes, which are fixed on shoulder joint and elbow joint by a pair of micro nozzles. These tubes are used to avoid air leakage and protect cables, which inner diameters are 1mm. Shoulder driven tubes and elbow driven tubes are connected to external driven tubes. The external driven tubes are connected to driven actuators. The arm can be moved by pulling six cables by driven actuators. Shoulder connector is used to connect the arm to the robot body. In addition, external tube can be very long, so driven actuators can be installed remotely, such as the bottom of the robot body as shown in Fig. 1. Air pressure is 7.32 ± 3.45 kPa in the robot arm. The arm merits of this novel soft inflatable arm is that, it combines the skin and framework as a whole, and very light, easy and low cost for fabrication. Meanwhile, most of the cables are wired inside the arm and make results in a tidy appearance. More detailed hardware designs are proposed in our another paper [12].

III. KINEMATIC MODELING

Modeling and kinematics in coordinate system for the soft inflatable arm are proposed as follows: Firstly, establish a 4DOF redundant rigid arm, and compute inverse kinematics by inputting the end effector position $P(x, y, z)$ and outputting joint angles $\Theta(\theta_1, \theta_2, \theta_3, \theta_4)$, where $P \in R$ and $\Theta \in R$. Secondly, establish joint models for the soft inflatable arm, where shoulder joint and elbow joint map to joint angles $\Theta_{12}(\theta_1, \theta_2)$ and $\Theta_{34}(\theta_3, \theta_4)$ in the rigid arm, respectively. The target of inverse kinematics for the soft joint is solved by inputting joint angles $\Theta_{12}(\theta_1, \theta_2)$ and $\Theta_{34}(\theta_3, \theta_4)$ and outputting shoulder cables length $L_{123}(l_1, l_2, l_3)$ and elbow cables length $L_{456}(l_4, l_5, l_6)$, respectively. Where $\Theta_{12} \in \Theta$, $\Theta_{34} \in \Theta$, $L_{123} \in R$, and $L_{456} \in R$. Finally, the performances of the soft inflatable arm are elevated by applying these algorithms.

A. Kinematics of 4DOF redundant rigid arm

As mentioned above, the input only has an end effector position $P(x, y, z)$, but need to get four joint angles $\Theta(\theta_1, \theta_2, \theta_3, \theta_4)$, so the system is redundant. We take the right arm as an example, and proposed the coordinate definition of the 4DOF redundant rigid arm is shown in Fig. 3. The standard DH (Denavit-Hartenberg) parameters are shown in Table 1. In Fig. 3, Coordinate system (X0,Y0,Z0) is fixed

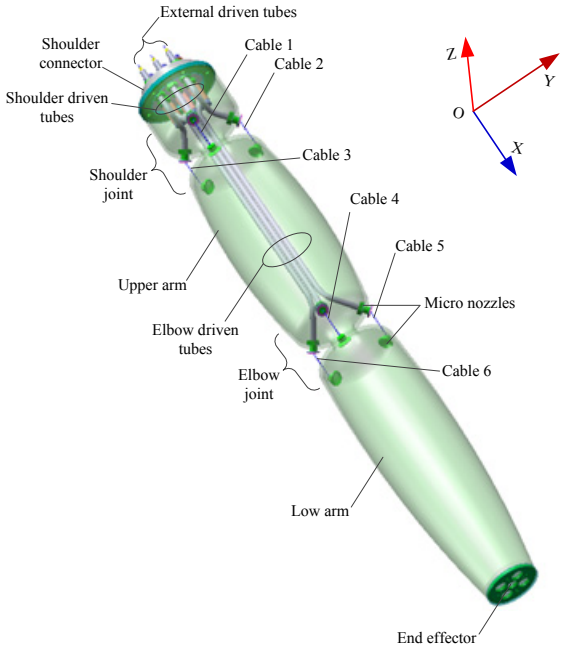

Fig. 2. The right soft inflatable arm

on robot body, and (X5,Y5,Z5) is the end effector of the right arm. l1 and l2 are the length of upper and lower arm, respectively. l1 and l2 both equal 190mm.

To calculate the inverse kinematics using geometrical method, we assume θ_3 is known, which is expressed as θ_{3f}. θ_{3f} $\left(\theta_{3f} \in \left[\begin{array}{cc} -\pi & \pi \end{array}\right]\right)$ is a variable using for motion planning, which follows as $\theta_{3f} = \sum_{-180}^{180} \frac{T\pi}{180}$, where T is a scale to calculate the kinematics. Hence, the problems will be simply as a 3DOF kinematics problem. The inverse kinematics will then be solved as follows. The different geometric projections for the 4DOF redundant rigid arm are shown Fig. 4. Plane X′OZ′ (shown in Fig. 4(c)) is a plane which equals plane X_0OZ_0 (shown in Fig. 4(a)) rotates along with axis OZ by angle θ_1.

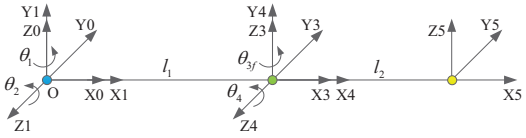

Fig. 3. Coordinate definition of the 4DOF redundant rigid arm

TABLE I
DH PARAMETERS OF THE 4DOF REDUNDANT RIGID ARM

θ_i(rad)	d_i(mm)	a_i(mm)	α_i(rad)
θ_1	0	0	$\frac{\pi}{2}$
θ_2	0	l_1	$-\frac{\pi}{2}$
θ_3	0	0	$\frac{\pi}{2}$
θ_4	d	l_2'	$-\frac{\pi}{2}$

In Fig. 4(a), we get $l_2' = l_2 \cos\theta_{3f}$, $d = l_2 \sin\theta_{3f}$, and $\theta_3 = \theta_{3f}$. In Fig. 4(b), we get $r = \sqrt{x^2 + y^2}$, $a = \sqrt{x^2 + y^2 - d^2}$, $\alpha = \tan^{-1}\left(\frac{d}{a}\right)$, and $\psi = \tan^{-1}\left(\frac{y}{x}\right)$. Combining these equations, we get

$$\theta_1 = \psi - \alpha \tag{1}$$

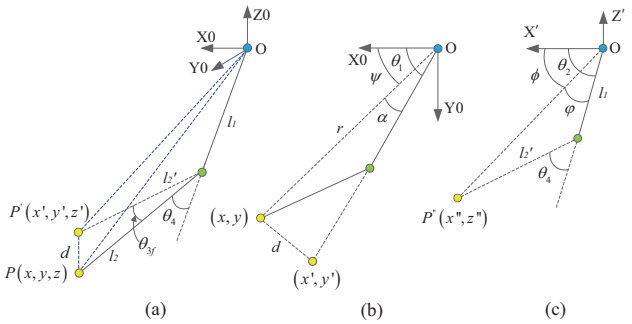

Fig. 4. Geometric projections for the 4DOF redundant rigid arm

Furthermore, in the Fig. 4(b) and Fig. 4(c) some equations will be calculated as below to get angle θ_2 and θ_4. Then we get $x' = a\cos\theta_1$, $y' = a\sin\theta_1$, $x'' = \sqrt{(x')^2 + (y')^2}$, and $z'' = z$.

$$\theta_4 = \pm 2\tan^{-1}\left(\sqrt{\frac{(l_1 + l_2')^2 - \left((x'')^2 + (z'')^2\right)}{\left((x'')^2 + (z'')^2\right) - (l_1 - l_2')^2}}\right) \quad (2)$$

There are two solutions of Eq. (2), and each solution is corresponding to a solution of θ_2. Then, $\phi = \tan^{-1}(z'', x'')$, $\varphi = \tan^{-1}(l_2' sin\theta_4, l_1 + l_2'\cos\theta_4)$. Then we get

$$\theta_2 = \phi - \varphi \quad (3)$$

Finally, the solution θ_1, θ_2, θ_3 and θ_4 are directly input into soft inflatable joint model to calculate cable length of shoulder and elbow, respectively. In addition, there may be other rigid arm configurations, but the above configuration and method are better and clearer for motion planning by planning θ_{3f} directly.

B. Modeling and kinematics of soft inflatable joint

As the shoulder joint is the same with the elbow joint, so we take the soft should joint as an instance to analyze. The actual inflatable joint and the proposed corresponding joint model are shown in Fig. 5(a) and Fig. 5(b), respectively, which also show the initial statement and coordinates definition. The following assumptions are made, three Cartesian coordinate systems (Xa,Ya,Za), (Xb,Yb,Zb), and (Xc,Yc,Zc) are attached to the fixed base, moving platform, and moving platform, respectively. Initially, coordinate systems (Xb,Yb,Zb), and (Xc,Yc,Zc) are coincided with (Xa,Ya,Za). Point P0 is located at the origination of fixed coordinate system (Xa,Ya,Za), and P_0 equals $[\ 0\quad 0\quad 0\ ]^T$. Points P_{a0} and P_{b0} are located at the centroid of $\triangle P_{a1}P_{a2}P_{a3}$ and $\triangle P_{b1}P_{b2}P_{b3}$, respectively. Radiuses of inscribed circles of $\triangle P_{a1}P_{a2}P_{a3}$ and $\triangle P_{b1}P_{b2}P_{b3}$ are r_a and r_b, respectively. The connections from point P_{a1} to P_{b1}, P_{a2} to P_{b2}, and P_{a3} to P_{b3} are corresponding to cable 1, cable 2 and cable 3, respectively. A cross-section plane C is fixed at moving coordinate system (Xc,Yc,Zc), which is the rotation plane of the joint. A circle C with radius r_c lies on plane C and its center point P_{c0} is coincided with P_0. Points P_{c1}, P_{c2} and P_{c3} are the intersections of plane C and cable1, cable2, cable3, respectively. And d_a and d_b equal $|P_0X_{a0}|$ and $|P_0X_{b0}|$, respectively. Coordinate systems (Xb,Yb,Zb) and (Xc,Yc,Zc) rotate with the fixed coordinate systems (Xa,Ya,Za) by θ_1 and θ_2 got from inverse kinematics in rigid arm above. The angle of direction of $\overline{P_0X_b}$ rotates with the direction of $\overline{P_0X_a}$ equals θ_1, and the angle of direction of $\overline{P_0Y_b}$ rotates with the direction of $\overline{P_0Y_a}$ equals θ_2. The angle of direction of $\overline{P_0X_c}$ rotates with the direction of $\overline{P_0X_a}$ equals $\theta_1/2$, and the angle of direction of $\overline{P_0Y_c}$ rotates with the direction of $\overline{P_0Y_a}$ equals $\theta_2/2$. These points can be expressed as ${}^aP_a = \begin{bmatrix} r_a & -\frac{r_a}{2} & -\frac{r_a}{2} \\ 0 & \frac{\sqrt{3}r_a}{2} & -\frac{\sqrt{3}r_a}{2} \\ -d_a & -d_a & -d_a \end{bmatrix}$ ${}^bP_b = \begin{bmatrix} r_b & -\frac{r_b}{2} & -\frac{r_b}{2} \\ 0 & \frac{\sqrt{3}r_b}{2} & -\frac{\sqrt{3}r_b}{2} \\ d_b & d_b & d_b \end{bmatrix}$ ${}^cP_c = \begin{bmatrix} r_c & -\frac{r_c}{2} & -\frac{r_c}{2} \\ 0 & \frac{\sqrt{3}r_c}{2} & -\frac{\sqrt{3}r_c}{2} \\ 0 & 0 & 0 \end{bmatrix}$. Where matrixes ${}^aP_a = [P_{a1}, P_{a2}, P_{a3}]$, ${}^bP_b = [P_{b1}, P_{b2}, P_{b3}]$ and ${}^cP_c = [P_{c1}, P_{c2}, P_{c3}]$ are the positions of in coordinate system (Xa,Ya,Za), (Xb,Yb,Zb), and (Xc,Yc,Zc), respectively. In addition, parameters r_a, r_b, r_c, d_a and d_b equal 35mm, 35mm, 20mm, 65mm,and 65mm, respectively, for the shoulder joint and elbow joint in the actual soft arm.

In the initial status (shown in Fig.5), θ_1 and θ_2 are both equal zero. But when θ_1 or θ_2 is varying, there will appear two situations, which are shown in Fig. 6. The actual inflatable joint and the proposed corresponding joint model are shown in Fig. 6(a) and Fig. 6(b), respectively. In Fig.6 (b), points P_{c1}, P_{c2} and P_{c3} are all outside circle C. In this case, θ_1 or θ_2 are generally small, and three cables can be calculated by as linear length. In this case, we call it Standard Soft Inflatable Joint Model (SSIJM). But when θ_1 or θ_2 are larger, points P_{c1}, P_{c2} or P_{c3} may be inside circle C, which is shown in Fig.6 (d). The actual inflatable joint and the corresponding joint model are shown in Fig. 6(c) and Fig. 6(d), respectively. In this situation, the corresponding cables should be processed as arcs. In this case, we call it Modified Soft Inflatable Joint Model (MSIJM).

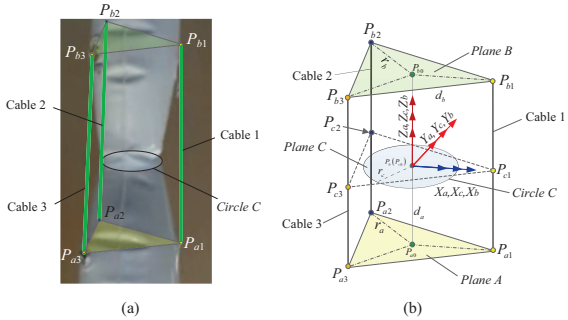

Fig. 5. Initial statement and coordinates definition for the shoulder joint

C. SSIJM kinematics

The target of SSIJM kinematics is to determine the length of three cables by giving θ_1 and θ_2. To simply calculation, let α and ϕ replace θ_1 and θ_2, respectively, which is shown in Fig. 7. α and ϕ can be calculated as following equations. We get $x_r = l_2 cos\theta_1 \sin\theta_2$, $y_r = l_2\sin\theta_1$, and $z_r = l_2 cos\theta_1\cos\theta_2$. Then,

$$\phi = \tan^{-1}(\frac{y_r}{x_r}) \quad (4)$$

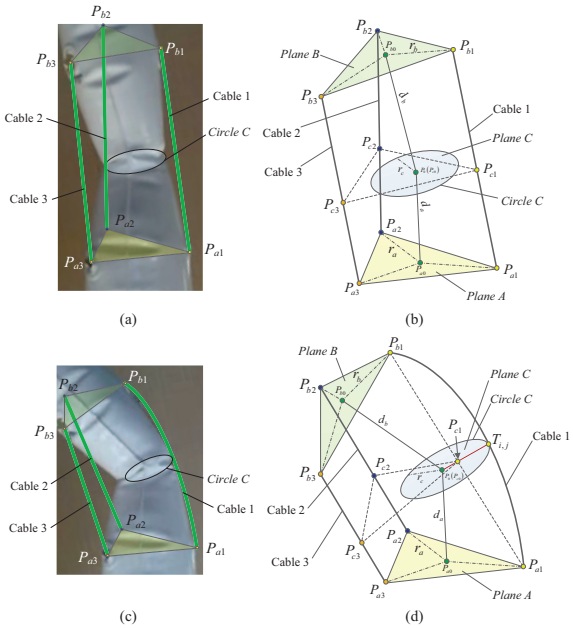

Fig. 6. Soft inflatable joint models

$$\hat{z}_r = x_r cos\phi + y_r sin\phi \tag{5}$$

$$\alpha = \tan^{-1}(\frac{\hat{z}_r}{z_r}) \tag{6}$$

The transformation from the fixed base (Xa,Ya,Za) to moving platform (Xb,Yb,Zb) and (Xc,Yc,Zc) can be described as follows,

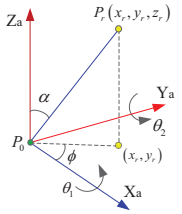

Fig. 7. Transformation from θ_1 and θ_2 to α and ϕ

$$^{a}R_b = Rotz(-\phi)Roty(\alpha)Rotz(\phi) \tag{7}$$

$$^{a}R_c = Rotz(-\phi)Roty(\frac{\alpha}{2})Rotz(\phi) \tag{8}$$

where $^{a}R_b$ and $^{a}R_c$ are the corresponding transformation matrixes. Then positions in moving platform (Xb,Yb,Zb) can be transferred to fixed base (Xa,Ya,Za) as $^{a}P_b$=$^{a}R_b$ $^{b}P_b$. Finally, the length of the three cables can be calculated as,

$$l_1 = \left\| (^{a}P_b - {}^{a}P_a)\begin{bmatrix} 1 & 0 & 0 \end{bmatrix}^T \right\| \tag{9}$$

$$l_2 = \left\| (^{a}P_b - {}^{a}P_a)\begin{bmatrix} 0 & 1 & 0 \end{bmatrix}^T \right\| \tag{10}$$

$$l_3 = \left\| (^{a}P_b - {}^{a}P_a)\begin{bmatrix} 0 & 0 & 1 \end{bmatrix}^T \right\| \tag{11}$$

where l_1, l_2 and l_3 are the length of cable 1, cable 2, and cable 3, respectively.

D. MSIJM kinematics

As mentioned above, the target of MSIJM kinematics is also to determine the length of three cables by giving θ_1 and θ_2. The kinematics problems can be solved by following steps.

1) Get intersections on the rotation center plane (plane C):: As shown in Fig. 5 and Fig. 6, positions in moving platform (Xc,Yc,Zc) can be transfer to fixed base (Xa,Ya,Za) by Eq. (8), then $^{a}P_c$=$^{a}R_c$ $^{c}P_c$. Let $\vec{v}_{12}$ and $\vec{v}_{13}$ are the different vectors between positions $(^{a}P_c)_{1,1}$ and $(^{a}P_c)_{1,2}$, and $(^{a}P_c)_{1,1}$ and $(^{a}P_c)_{1,3}$, respectively. The intersection plane can be calculated as $\vec{v}_{12} = (^{a}P_c)_{1,1} - (^{a}P_c)_{1,2}$ and $\vec{v}_{13} = (^{a}P_c)_{1,1} - (^{a}P_c)_{1,3}$. Then the normal vector of $\vec{v}_{12}$ and $\vec{v}_{13}$ follow as $\vec{n}_{ac} = \vec{v}_{12} \times \vec{v}_{13}$.

The next step is to get the intersections between the plane C and the three cables we just calculated by SSIJM kinematics above, which follows as,

$$u_{i,1} = \left(\vec{n}_{ac}\right)_{1,1} L_{1,j} + \left(\vec{n}_{ac}\right)_{2,1} L_{2,j} + \left(\vec{n}_{ac}\right)_{3,1} L_{3,j} \tag{12}$$

where $i \in [1,3]$ and $j \in [1,3]$. Then

$$w_{i,1} = \frac{\left((P_0)_{1,1} - \left(^{a}P_a\right)_{1,j}\right)\left(\vec{n}_{ac}\right)_{1,1} + \left((P_0)_{2,1} - \left(^{a}P_a\right)_{2,j}\right)\left(\vec{n}_{ac}\right)_{2,1} + \left((P_0)_{3,1} - \left(^{a}P_a\right)_{3,j}\right)\left(\vec{n}_{ac}\right)_{3,1}}{u_{i,1}} \tag{13}$$

where $i \in [1,3]$ and $j \in [1,3]$. Finally, the intersections of the plane C and the three cables can be computed as,

$$Q = {}^{a}P_a + L^T \begin{bmatrix} w_{1,1} & 0 & 0 \\ 0 & w_{2,1} & 0 \\ 0 & 0 & w_{3,1} \end{bmatrix} \tag{14}$$

where Q is an assumed matrix to replace points P_{c1}, P_{c2} and P_{c3}. In addition, when $u_{i,j}$ equals zero, the corresponding column items of matrix Q is null. The next step is to calculate the length between the point P_0 to three intersections, which are follow as,

$$\hat{r}_{i,1} = \left(\begin{matrix} \left(Q_{1,j} - (P_0)_{1,1}\right)^2 + \left(Q_{2,j} - (P_0)_{2,1}\right)^2 \\ + \left(Q_{1,j} - (P_0)_{3,1}\right)^2 \end{matrix} \right)^{1/2} \tag{15}$$

where $i \in [1,3]$ and $j \in [1,3]$. When $\hat{r}_{i,1}$ is no more than r_c (as shown in Fig. 6), the corresponding cable length will be calculated as a length of the arc.

2) Get intersections direction:: The next step is to calculate the intersections between P_0 and the intersection plane C, $\hat{r}_{i,1}$ is no more than r_c. Let points Q_1, Q_2 and Q_3 are the column items of matrix, then the intersection on the arc will follows as,

$$M_{i,j} = Q_{i,j} - (P_0)_{i,1} \tag{16}$$

If $\|M_{i,j}\| \neq 0$, then

$$N_{i,j} = \frac{r_c M_{i,j}}{\|M_{i,j}\|} + (P_0)_{i,1} \tag{17}$$

where point $N_{i,j}$ is a temporary intersection on the arc. Actually, there are one solution and another solution show in Fig. 6 and Fig. 8, respectively. The former one is the desired solution. A new method is shown in Fig.9 used to judge the intersection direction. We assume point $N_{i,j}$ the desired solution, and then verify it as follows.

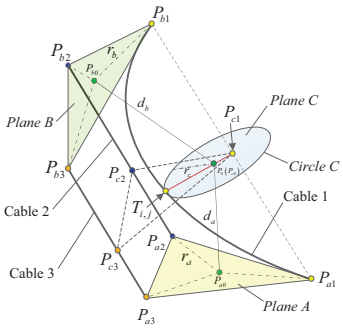

Fig. 8. The other solution of intersection direction

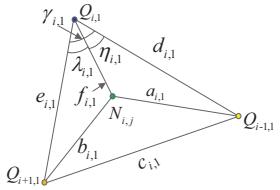

Fig. 9. Diagram of judging intersection direction

$$a_{i,1} = \left(\begin{array}{c} (Q_{i-1,1} - N_{i,1})^2 + (Q_{i-1,2} - N_{i,2})^2 \\ +(Q_{i-1,3} - N_{i,3})^2 \end{array} \right)^{1/2} \quad (18)$$

$$b_{i,1} = \left(\begin{array}{c} (Q_{i+1,1} - N_{i,1})^2 + (Q_{i+1,2} - N_{i,2})^2 \\ +(Q_{i+1,3} - N_{i,3})^2 \end{array} \right)^{1/2} \quad (19)$$

$$c_{i,1} = \left(\begin{array}{c} \left(Q_{i+1,1} - Q_{i-1,1}\right)^2 + \left(Q_{i+1,2} - Q_{i-1,2}\right)^2 \\ +\left(Q_{i+1,3} - Q_{i-1,3}\right)^2 \end{array} \right)^{1/2} \quad (20)$$

$$d_{i,1} = \left(\begin{array}{c} (Q_{i-1,1} - Q_{i,1})^2 + (Q_{i-1,2} - Q_{i,2})^2 \\ +(Q_{i-1,3} - Q_{i,3})^2 \end{array} \right)^{1/2} \quad (21)$$

$$e_{i,1} = \left(\begin{array}{c} (Q_{i+1,1} - Q_{i,1})^2 + (Q_{i+1,2} - Q_{i,2})^2 \\ +(Q_{i+1,3} - Q_{i,3})^2 \end{array} \right)^{1/2} \quad (22)$$

$$f_{i,1} = \left(\begin{array}{c} (Q_{i,1} - N_{i,1})^2 + (Q_{i,2} - N_{i,2})^2 \\ +(Q_{i,3} - N_{i,3})^2 \end{array} \right)^{1/2} \quad (23)$$

$$\gamma_{i,1} = \arccos\left(\frac{d_{i,1}^2 + e_{i,1}^2 - c_{i,1}^2}{2d_{i,1}e_{i,1}}\right) \quad (24)$$

$$\eta_{i,1} = \arccos\left(\frac{d_{i,1}^2 + f_{i,1}^2 - a_{i,1}^2}{2d_{i,1}f_{i,1}}\right) \quad (25)$$

$$\lambda_{i,1} = \arccos\left(\frac{e_{i,1}^2 + f_{i,1}^2 - b_{i,1}^2}{2e_{i,1}f_{i,1}}\right) \quad (26)$$

where $i \in [1,3]$ and $j \in [1,3]$. The coefficient to judge the directions for the intersection on the arc is computed as,

$$\begin{cases} k = 1 & (\gamma_{i,1} > \lambda_{i,1} + \eta_{i,1}) \\ k = -1 & (\gamma_{i,1} \le \lambda_{i,1} + \eta_{i,1}) \end{cases} \quad (27)$$

Finally, the point on the arc will be calculated as,

$$T_{i,j} = \frac{kr_c M_{i,j}}{\|M_{i,j}\|} + (P_0)_{i,1} \quad (28)$$

And $T_{i,j}$ is the real solution to replace $N_{i,j}$. Moreover, when $\|M_{i,j}\| = 0$, there are infinite solutions.

3) Get the modified cable:: The next step is to calculate the modified cable which is shown in Fig. 10. From the above positions $({}^aP_b)_{i,j}$, $({}^aP_a)_{i,j}$ and $T_{i,j}$, and $\triangle({}^aP_b)_{i,j}({}^aP_a)_{i,j}T_{i,j}$ assumed in plane H. Then,

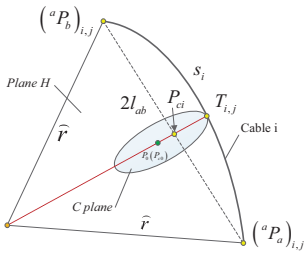

Fig. 10. Diagram for the modified cable

$A = \left[\begin{array}{ccc} A_1 & A_2 & A_3 \end{array} \right]^T$, $B = T_{i,j} - ({}^aP_b)_{i,j}$, $C = ({}^aP_a)_{i,j} - ({}^aP_b)_{i,j}$, and $D = \left[\begin{array}{ccc} D_1 & D_2 & D_3 \end{array} \right]^T$, where

$$\begin{aligned} A_1 = & \left({}^aP_b\right)_{2,j} T_{3,j} - \left({}^aP_b\right)_{2,j}\left({}^aP_a\right)_{3,j} - \left({}^aP_b\right)_{3,j} T_{2,j} \\ & + \left({}^aP_b\right)_{3,j}\left({}^aP_a\right)_{2,j} + \left({}^aP_a\right)_{3,j} T_{2,j} - \left({}^aP_b\right)_{2,j} T_{3,j} \end{aligned}$$

$$\begin{aligned} A_2 = & -\left({}^aP_b\right)_{1,j} T_{3,j} + \left({}^aP_b\right)_{1,j}\left({}^aP_a\right)_{3,j} + \left({}^aP_b\right)_{3,j} T_{1,j} \\ & - \left({}^aP_b\right)_{3,j}\left({}^aP_a\right)_{1,j} - \left({}^aP_a\right)_{3,j} T_{1,j} + \left({}^aP_a\right)_{1,j} T_{3,j} \end{aligned}$$

$$\begin{aligned} A_3 = & \left({}^aP_b\right)_{1,j} T_{2,j} - \left({}^aP_b\right)_{1,j}\left({}^aP_a\right)_{1,j} - \left({}^aP_b\right)_{2,j} T_{1,j} \\ & + \left({}^aP_b\right)_{2,j}\left({}^aP_a\right)_{1,j} + \left({}^aP_a\right)_{2,j} T_{1,j} - \left({}^aP_a\right)_{1,j} T_{2,j} \end{aligned}$$

$$\begin{aligned} D_1 = & -\left({}^aP_b\right)_{1,j}\left({}^aP_a\right)_{3,j} T_{2,j} + \left({}^aP_b\right)_{1,j}\left({}^aP_a\right)_{2,j} T_{3,j} \\ & + \left({}^aP_b\right)_{2,j}\left({}^aP_a\right)_{3,j} T_{1,j} - \left({}^aP_b\right)_{2,j}\left({}^aP_a\right)_{1,j} T_{3,j} \\ & - \left({}^aP_b\right)_{3,j}\left({}^aP_a\right)_{2,j} T_{1,j} + \left({}^aP_b\right)_{3,j}\left({}^aP_a\right)_{1,j} T_{2,j} \end{aligned}$$

$$D_2 = \left({}^aP_b\right)_{1,j}^2 + \left({}^aP_b\right)_{2,j}^2 + \left({}^aP_b\right)_{3,j}^2 - T_{1,j}^2 - T_{2,j}^2 - T_{3,j}^2$$

$$\begin{aligned} D_3 = & \left({}^aP_b\right)_{1,j}^2 + \left({}^aP_b\right)_{2,j}^2 + \left({}^aP_b\right)_{3,j}^2 - \left({}^aP_a\right)_{1,j}^2 \\ & - \left({}^aP_a\right)_{2,j}^2 - \left({}^aP_a\right)_{3,j}^2 \end{aligned}$$

Where $i \in [1,3]$ and $j \in [1,3]$. Then, the matrix of arc center position E can be computed as,

$$E = -\left(\left[\begin{array}{ccc} A & 2B & 2C \end{array} \right]^T\right)^{-1} D \quad (29)$$

And the radius of the arc can be computed as,

$$\widehat{r} = \left(\begin{array}{c} \left(\left({}^aP_b\right)_{1,j} - E_{1,j}\right)^2 + \left(\left({}^aP_b\right)_{2,j} - E_{2,j}\right)^2 \\ +\left(\left({}^aP_b\right)_{3,j} - E_{3,j}\right)^2 \end{array} \right)^{1/2} \quad (30)$$

In addition, the half-length between point $({}^aP_b)_{i,j}$ and point $({}^aP_a)_{i,j}$ can be computed as,

$$l_{ab} = \frac{1}{2}\left(\begin{array}{c} \left(\left({}^aP_b\right)_{1,j} - \left({}^aP_a\right)_{1,j}\right)^2 + \left(\left({}^aP_b\right)_{2,j} \\ - \left({}^aP_a\right)_{2,j}\right)^2 + \left(\left({}^aP_b\right)_{3,j} - \left({}^aP_a\right)_{3,j}\right)^2 \end{array} \right)^{1/2} \quad (31)$$

Finally, the modified arc length will be calculated as,

$$s_i = 2\widehat{r}\arcsin\left(\frac{l_{ab}}{\widehat{r}}\right) \quad (32)$$

where $i \in [1,3]$. The compounding length of the cable l_i will be replaced by s_i, when are intersections (points P_{c1}, P_{c2} or P_{c3} may be inside circle C).

4) Elbow joint kinematics:: For elbow joint, the target is to solve inputting θ_3 and θ_4, and outputting three cables on elbow joint. These cables can be easily calculated by replacing θ_1 and θ_2 to θ_3 and θ_4 by using Eq. (4) $\sim$ Eq. (32), respectively. But there is a rotation offset between elbow joint and shoulder joint, which follows as $\tilde{x} = ({}^aP_b)_{1,1}\cos\theta_2 + ({}^aP_b)_{2,1}\sin\theta_1\sin\theta_2 - ({}^aP_b)_{3,1}\cos\theta_1\sin\theta_2$, $\tilde{y} = ({}^aP_b)_{2,1}\cos\theta_1 + ({}^aP_b)_{3,1}\sin\theta_1$, $\tilde{l} = \sqrt{\left(({}^bP_b)_{1,1} - \tilde{x}\right)^2 + \left(({}^bP_b)_{2,1} - \tilde{y}\right)^2}$, $\xi = 2\arcsin\left(\frac{\tilde{l}}{r_a}\right)$, and $\tau = ({}^bP_b)_{1,1}\tilde{y} - \tilde{x}({}^bP_b)_{2,1}$. Then, the offset ξ will be modified as,

$$\xi = \begin{cases} -2\arcsin\left(\frac{\tilde{l}}{r_a}\right) & (\tau < 0) \\ 2\arcsin\left(\frac{\tilde{l}}{r_a}\right) & (\tau > 0) \end{cases} \tag{33}$$

where τ is used to determine the rotation direction. Finally, the offset ξ will add the rotation to elbow joint to match the posture of rigid arm. For the elbow joint, a new ϕ in Eq. (4) will be modified as,

$$\phi = a\tan 2(y_r, x_r) + \xi \tag{34}$$

Meanwhile this method can be applied to more than two joint by compensating ϕ in Eq. (34).

IV. EXPERIMENTS AND RESULTS

To verify the kinematics model of the soft inflatable arm, numerous experiments are carried out. The right soft inflatable arm moves in X, Y, and Z direction are shown in Fig. 11, Fig. 12, and Fig. 13, respectively. All these experiments follow the rule that when one directional position of the end effector varies, the other two directional positions will be fixed. The drawn horizontal and vertical lines in the figures are used to compare the desired and actual positions.

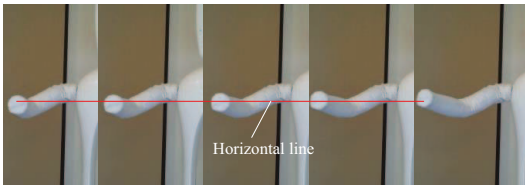

Fig. 11. Soft inflatable arm moves in X direction

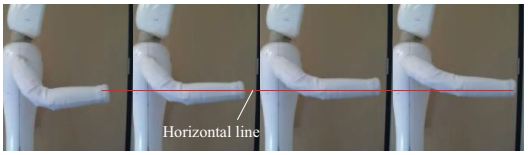

Fig. 12. Soft inflatable arm moves in Y direction

The experimental results show that the positioning accuracy in X, Y, and Z directions are 33.906mm, 34.213mm, and 29.435mm, respectively, which are the mean values of differences between desired positions and actual positions of end effector. Also, numerous experimental results show that the end effector workspace in coordinate systems follows $x \in [0, 380]$, $y \in [0, 370]$ and $z \in [0, 360]$, and the maximum velocity is about 250mm/s, which are close to an adults arm movement space and normal motion speed [13-14].

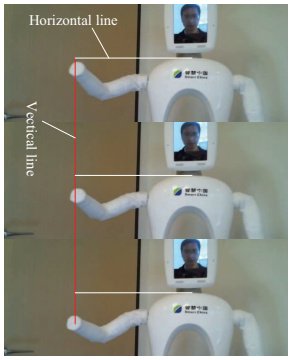

Fig. 13. Soft inflatable arm moves in Z direction

V. CONCLUSIONS AND FUTURE WORK

In conclusion, in this paper the challenge problems of kinematic modeling and control for a multi-joint inflatable robot arm with cable-driven mechanism are proposed and solved, including modeling and kinematics of redundant rigid arm and soft inflatable joint. These models and algorithms can be applied to muti-joint soft inflatable arms with less pressure and lighter weight. Numerous experiments have been conducted, including movement space and positioning accuracy in Three-Dimensional coordinate system. The soft inflatable robot arm is also capable of imitating human arms to realize remote interaction. In the future, more experiments and performances of kinematics and dynamics will be implemented and evaluated.

REFERENCES

[1] Antonio Bicchi and Giovanni Toniett, IEEE Robotics and Automation Magazine,June 2004, pp: 22-33.

[2] S. Haddadin, A. Albu-Schaffer, and G. Hirzinger, Safety evaluation of physical human-robot interaction via crash testing, Robot. Sci. Syst. Conf., 2007.

[3] K. Ikuta, H. Ishii, and M. Nokata, Safety evaluation method of design and control for human-care robots, Int. J. Robot. Res., vol. 22, no. 5, May 2003, pp. 281C297.

[4] Yoram Koren, Ann Arbor, Yiechiel Weinstein Misgav, Inflatable structure, US Patent 5065640.

[5] R. Baldur and W. Blach, Inflatable manipulator, Society of Manufacturing Engineers, 1985.

[6] S. Voisembert, A. Riwan and N. Mechbal, Numerical Evaluation of a New Robotic Manipulator based on Inflatable Joints., 8th IEEE International Conference on Automation Science and Engineering, August 20-24, 2012, Seoul, Korea, pp: 544-549.

[7] Siddharth Sanan, Soft Robots for Safe Physical Human Interaction, PHD thesis.

[8] Siddharth Sanan, Michael H. Ornstein and Christopher G. Atkeson, Physical Human Interaction for an Inflatable Manipulator, 33rd Annual International Conference of the IEEE EMBS Boston, Massachusetts USA, August 30 - September 3, 2011, pp: 7401-7404.

[9] Siddharth Sanan, Justin B. Moidel and Christopher G. Atkeson, Robots with Inflatable Links, The 2009 IEEE/RSJ International Conference on Intelligent Robots and Systems, October 11-15, 2009, St. Louis, USA, pp: 4331-4336.

[10] Otherlab, https://otherlab.com/.

[11] Saul Griffith, Otherlab, https://otherlab.com/.

[12] Ronghuai Qi, Tin Lun Lam, and Yangsheng Xu, Mechanical Design and Implementation of a Soft Inflatable Robot Arm for Safe Human−Robot Interaction, 2014 IEEE International Conference on Robotics and Automation, May 31 - June 7, 2014, Hong Kong, China.

[13] H. Nagasaki, Asymmetric velocity and acceleration profiles of human arm movements, Exp Brain Res (1989)74, pp: 319-326.

[14] H I Krebs, N Hogan, M L Aisen, B T Volpe, Quantization of Continuous Arm Movements in Humans with Brain Injury, Proc. Nat. Acad. of Science 1999(96), pp: 4645-4649.